2D Magnetic Sensor Array for Real-time Cell Tracking and Multi-site Detection with Increased Robustness and Flow-rate

Hao Tang¹, Suresh Venkatesh¹, Zhongtian Lin², Xuyang Lu¹, Hooman Saeidi¹, Gulam M. Rather³, Joseph R. Bertino³, Chen-Yong Lin⁴, Mehdi Javanmard², and Kaushik Sengupta¹

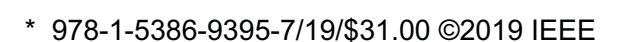
Abstract—In this article, we present a 2D oscillator array-based magnetic sensor CMOS IC for flow cytometry. The CMOS IC packaged with a microfluidic channel eliminates the need for hydro-focusing by allowing uninhibited flow over the 2D chip surface. The chip exploits multi-site detection capability allowing simultaneously high flow rate for trace cell detection, reduced false positives, and real-time cell tracking. We demonstrate these functionalities with a 7×7 array in 65-nm CMOS with lymphoma cancer cells.

I. INTRODUCTION

Magnetic detection in flow cytometry is emerging as an alternative to optical based detection mechanisms due to the ability to integrate such magnetic sensors in chip-scale platform, overcoming the limitations of complex and bulky optical instrumentation and fluorescence labeling [1], [2], [3]. Such flow cytometers are particularly useful for detecting trace cancer cells and circulating tumor cells that naturally shed from the primary site, and can circulate in the blood stream leading to new metastasis [4]. Robust detection of such cells can allow early diagnosis of cancers, examination of cancer relapse and recurrence, and evaluating efficiency of chemotherapeutic interventions. However, this is particularly difficult given the trace nature of these cells (1 in 0.1-1 million healthy cells), and therefore, point-of-care platforms are essential to ensure large flow rates with extremely low false probabilities. Classical magnetic-based flow cytometers typically employ a single sensor and hydro-focuses the flow to ensure that all cells flow over the sensor to avoid missing the detection of the trace cells. This approach creates two issues. Firstly, reliance on one sensor creates the issue of false or missed detection, and the resultant false positives and false negatives. Optical-based detection tries to overcome these issues with multiple orthogonal measurements from scattering cross section areas to florescence emissions. Secondly, concentrating the flow on one sensor reduces the volume rate of analysis per minute which is particularly detrimental in cell detection in such cytometer applications.

In this paper, we address this in an approach that relies on multi-sensor processing in an array of 2D magnetic sensors in CMOS that 1) allows the volume to flow on the entire 7×7 array of oscillator-based sensors (instead of focusing) leading to high volume rate 2) relies on detection of the magnetically labeled cells across multiple sites in a time progressive manner as the sample flows over the array leading

 $^{^1\}mathrm{Department}$ of Electrical Engineering, Princeton University, $^2\mathrm{Department}$ of Electrical and Computer Engineering, Rutgers University, $^3\mathrm{Rutgers}$ Cancer Institute of New Jersey, and 4 Department of Oncology, Georgetown University.



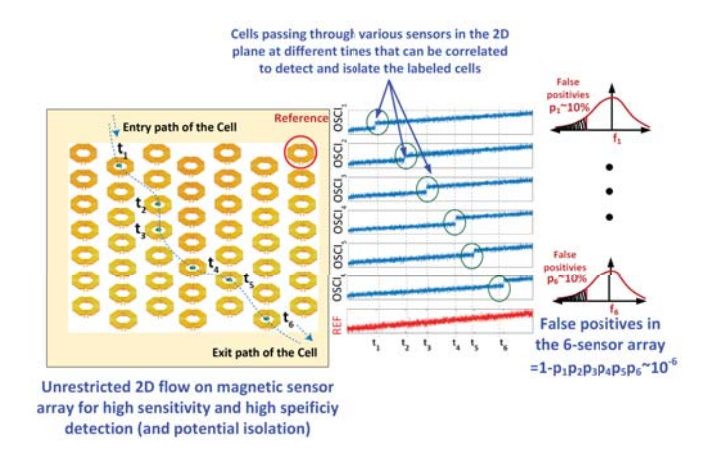


Fig. 1. Concept of the 2D magnetic sensor array allowing real-time cell tracking, increased flow rates and reduced false detection probabilities.

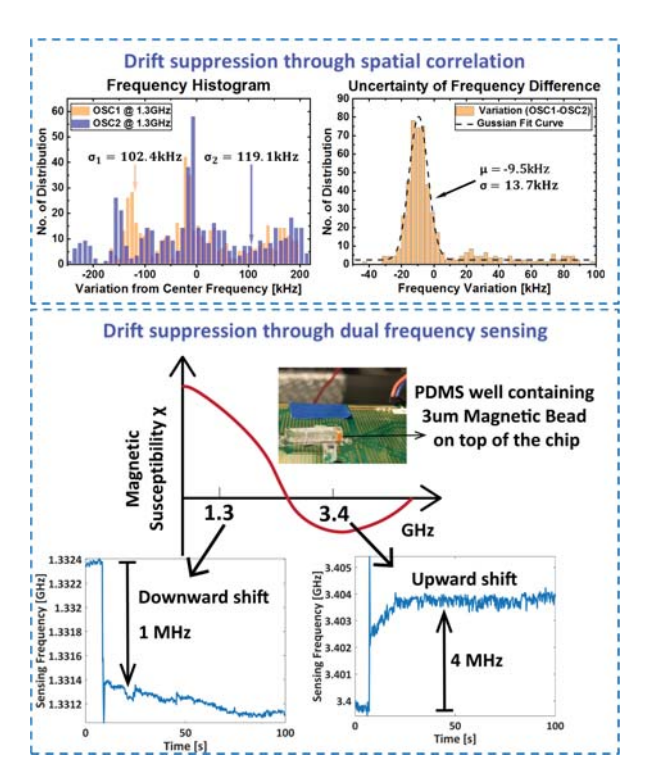


Fig. 2. Figure shows exploitation of oscillator drift correlation to increase specificity and dual frequency measurement to minimize single pixel drift.

to much higher robustness and order of magnitude lower false detection 3) exploits correlated low-frequency drifts across the multiple oscillator-sensor pixels due to correlated temperature change and voltage fluctuations across the array to allow higher specificity detection 4) encompasses a dual modality of detection at 1.3 GHz and 3.4 GHz (where the employed magnetic beads reverses its response) to suppress single-pixel drifts and 5) employs a staggered layout to ensure no cells are missed during the detection process.

II. MAGNETIC SENSOR ARRAY AND HIGH-SPECIFICITY DETECTION IN UNRESTRICTED FLOWS

The concept is illustrated in Fig. 1 and 2. As the sample is allowed to flow over the 2D array, the magnetically labeled cell will create perturbations in the field across multiple sensing sites in a time-progressive manner dependent on the flow rate and this is key to robust detection. Therefore, single site perturbation without progressive sensing at the neighboring sites can be constituted as a false positive. It can be noted that the exact rate of the flow is not needed to be known beforehand, and detection algorithms that search for the perturbation within a time window can be easily incorporated. The 2D array not only allows such multiple detection schemes and a larger flow rate, but can also support an arbitrary flow of the sample under fast turbulent rates, and relies on back-end signal processing to extract the bead path.

A. Drift suppression through spatial correlation and frequency switching

In the work, we employ CMOS-based LC oscillators as the magnetic sensor core [5]. However, the specificity of each oscillator to sense the local perturbations in such flowbased measurements are typically limited by the oscillator drifts as opposed to the higher frequency phase noise of the oscillators in magnetically-labeled assay-based detection. This is due to the time constants involved in these magnetic measurements of cytometers. As an example, in a moderately high flow rate of 10 mm/s, a cell will take 16 ms to flow over a 160 μ m diameter oscillator coil. The frequency shift in such a time frame is related to the low frequency drifts of the oscillator typically due to correlated temperature and supply voltage fluctuations, across all sensors of the array. This is shown in Fig. 2, where the variance of the difference of two oscillators with a correlation coefficient (ρ_{corr} =0.98) collapses the frequency uncertainty within the measurement time-period by 7.5×. Further enhancement of the sensor can be achieved by comparing a pixel with itself by switching fast between the two frequencies of 1.3 GHz and 3.4 GHz, the latter where the magnetic bead susceptibility reverses in sign. This results in an upward shift of the oscillator frequency as shown in Fig. 2.

The presented CMOS-based magnetic sensor array integrates a 49-sensor array where any two oscillators can be addressed simultaneously by choosing either frequency of oscillation (1.3 GHz and 3.4 GHz) in either of them. For the 3.4 GHz chosen output, the IC also has an integrated divide-by-3 frequency divider, to mix with the 1.3 GHz signal and cancel the drift partially on-chip. The correlation of the two measured oscillators at 1.3 GHz and 3.4GHz is exploited to further enhance sensor specificity during detection.

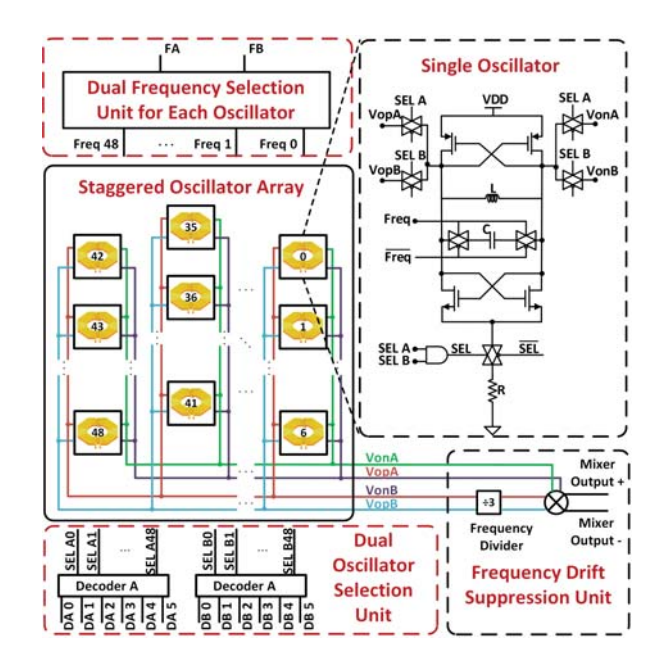


Fig. 3. Architecture of the 7x7 sensor array with independent and dual sensor and frequency selection capability allowing real-time tracking of the magnetically-labeled cells.

B. CMOS Magnetic Sensor Array and Oscillator Design

The architecture of the oscillator-based sensor array is illustrated in Fig. 3. The sensors are laid out in a staggered fashion to allow coverage of the magnetic sensing plane and avoid missing a cell passing between two sensors. Each sensor comprises of a digitally controlled oscillator capable of oscillating at 1.3 GHz and 3.4 GHz. The core of the oscillator is realized with cross-coupled NFET and PFET pairs. In order to minimize DC power consumption to maintain a constant chip surface temperature, only two oscillators are switched on at any given moment (at either of the two states) and they can be read simultaneously.

As shown in Fig. 3, the dual frequency selection unit sets the frequency of these two selected oscillators to either 1.3 GHz or 3.4 GHz. The drift cancellation unit also consists of a frequency divider (by 3) followed by a passive mixer. Each oscillator output prior to the drift cancellation unit is also tapped out. All the control/selection units mentioned above are controlled through an external FPGA board to dynamically program and to scan the pixels.

The schematic of the single sensor pixel is shown in Fig. 4. The on-chip inductor is realized on 3.4 μ m copper thickness and has a simulated inductance of 3.8 nH, and a quality factor of 10 at 1.3 GHz. Fig. 4 also shows the simulated fractional inductance change due to a single bead as a function of the distance from the sensor for 1 μ m bead. We perform a full-wave electromagentic simulation to capture the frequency change due to a 1 μ m diameter magnetic bead. This leads to an approximate frequency change of about 300 Hz. Hence a single 3 μ m bead can lead to an 8.1 kHz change in oscillation frequency (due to increase in volume). Fig. 4 shows a simulated phase noise value of -121 dBc/Hz at a 1 MHz offset. The figure also shows the measured distribution

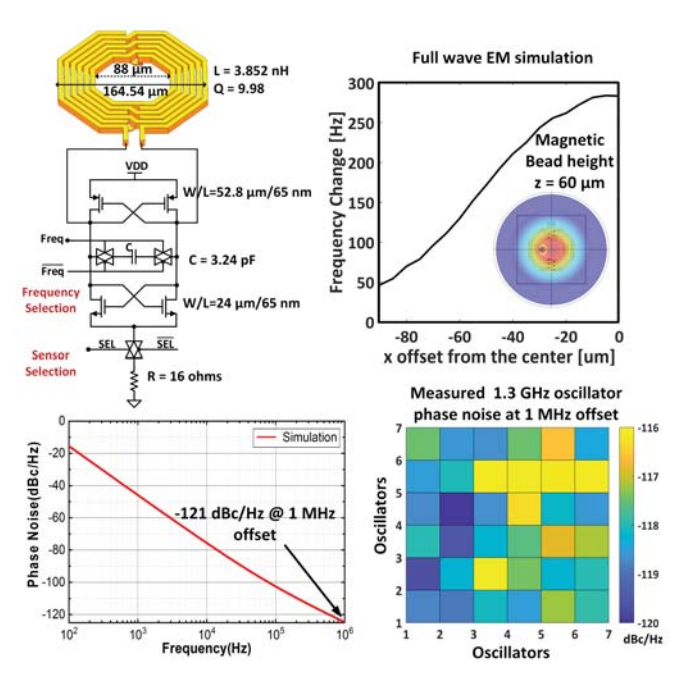


Fig. 4. Single pixel oscillator circuit diagram with simulated frequency change responsivity due to a magnetic particle. The figure also shows phase noise simulation and measured phase noise of all 1.3 GHz oscillators at 1 MHz offset.

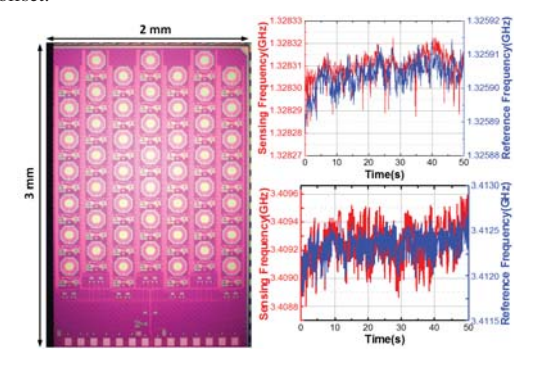


Fig. 5. Chip micrograph and measured frequency drifts of two selected oscillators at 1.3 GHz and 3.4 GHz showing the correlation effects due to temperature and supply voltage uctuations

of phase noise at 1 MHz offset of the 2D sensor array.

III. MEASUREMENT RESULTS

The chip is fabricated in a 65-nm bulk CMOS process. The chip micrograph is shown in Fig. 5. The chip measures 2 mm ×3 mm in size. Firstly, we characterize an individual pixel for its short and long time drifts and investigate correlation across multiple sensors distributed over the chip. The figure shows the measured frequency drifts of two selected oscillators at 1.3 GHz and 3.4 GHz showing the correlation effects due to temperature and supply voltage fluctuations. The measured phase noise of a representative oscillator is shown in Fig. 6a. The measured phase noise at 1.3 GHz is at -120 dBc/Hz at 1 MHz offset and the distribution of the phase noise over the sensor array is shown in Fig. 4. To better understand, the correlation across the 2D array, we measured the correlation of multiple sensors across the array. As can be

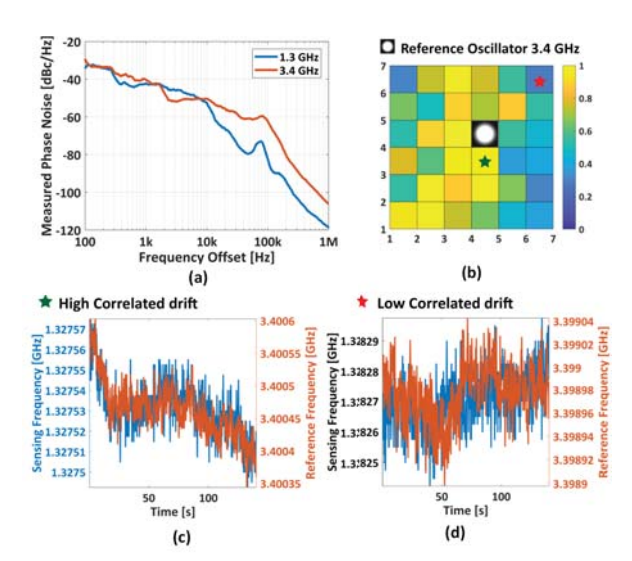


Fig. 6. (a) Measured phase noise (b)-(d) Measured correlation of the oscillator array across space across a high and a low correlation site.

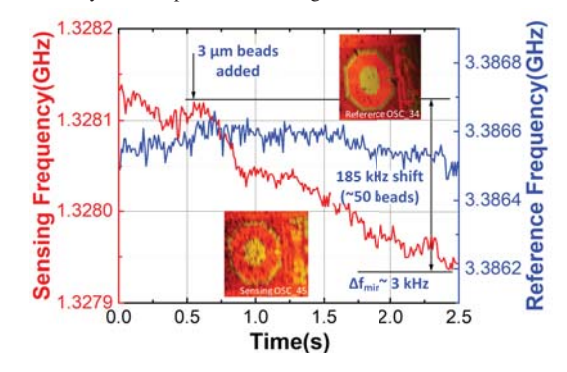


Fig. 7. Measured frequency response of the sensor pixel (and the reference pixel) as approximately 50 beads descend from the sample surface on to the sensor surface over a period of 1 second.

seen from Fig. 6c-d, the correlation has a spatial dependence and therefore, the reference and sensor oscillators need to be chosen to allow correlated variations to dominate the drift. This is particularly true for flow measurements, where the surrounding environment can strongly affect the drift of the individual sensors.

The sensor is then tested with magnetic beads that are used for labeling of the cancer cells in the biosensor measurements. The sensor response to 3 μ m superparamagnetic beads (ProMag 3 HP) is measured by allowing the beads to settle on the sensor surface (Fig. 7). The measured sensor and reference response shows the gradual frequency drift as all the beads settle on the surface over a period of 2 seconds. The measured frequency shift of 185 kHz for around 50 such beads leads to a frequency change of \sim 3.7 kHz/bead.

Following that, the sensor is measured with cultured lympohoma cancer cells which are bonded with the 2.8 μ m super-paramagnetic Dynabeads (M-280) with an antimatriptase monoclonal antibody (M69) and an IgG-magnetic bead assembly. The measured sensor response when a cancer cell is placed with a celltram vario (Eppendorf) is shown in Fig. 8. The change in the frequency response after the cell

Metrics	Ref [6]	Ref [4]	Ref [1]	This work
Technology	PHEMT	GMR	65 nm CMOS	65 nm CMOS
No. Sensors	8	4	2	49 (reduced false positives & high flow rate)
Sensor	24 μHall detector	GMR	Spiral transformer	LC tank
Sensor Integration	N/A	N/A	On-chip	On-chip
Sensing Area	N/A	N/A	1.3 mm ²	3.6 mm ²
Excitation Field	DC	DC	0.9 GHz & 2.6 GHz	1.3 GHz & 3.4 GHz
Frequency				
Other Component	0.5 T magnet	0.2 T magnet	10 mT magnet	None
Detection Time	0.02 ms	40 ms	10 ms	10 ms
Throughput	N/A	24 μ L/min	$2.4~\mu$ L/min	36 μ L/min (10mm/sec flow)

TABLE I

COMPARISON TABLE OF DIFFERENT FLOW CYTOMETRY TECHNIQUES REQUIRING MAGNETIC LABELS.

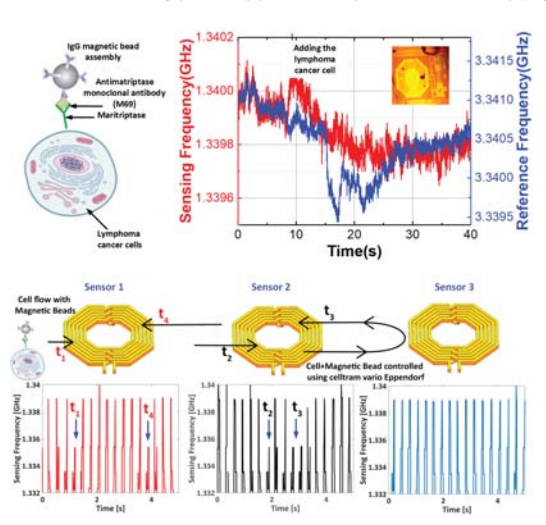


Fig. 8. Measured response of the sensor pixel and the reference when a lymphoma cancer cell cluster with magnetic bead is added to the system. The figure also shows the tracking with sequential frequency perturbation as the cancer cell transits across the chip allowing real-time tracking and reduced false positive detections.

is added is evident from the response. To demonstrate the real-time cell tracking ability exploiting multiple sensors, we allow the cells to pass over the chip through microfluidic trench packaged with a CMOS chip and controlled with the celltram vario. As the cell cluster passes through Sensor1-to-Sensor2 and back to Sensor 1 sequentially, the sensors are activated at a rate of 100 ms. We see the expected reduction in frequency at the exact time when the cell cluster passes over the array. This can be done across the 2D array to allow real-time 2D cell tracking, and multiple site detections to minimize false positives in a high throughput flow. The comparison table for different flow cytometry techniques is shown in Table I.

The presented work has the capability of employing a 2D array of sensors with no external magnets that allow simultaneously high flow rates, high sensitivity and high specificity (reduction of false positives). The measurement setup which includes the microfluidic channel on the IC along with the cell manipulation system is shown in Fig. 9.

ACKNOWLEDGMENT

We acknowledge the support of National Science Foundation, Princeton Catalysis Initiative, Princeton Intellectual Property Fund, and Princeton Bartlett Fund. We also thank

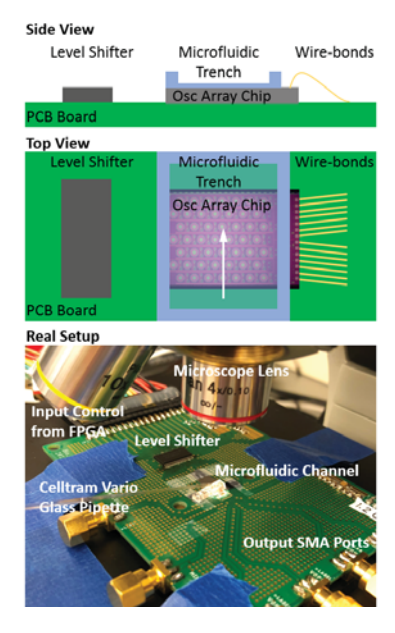


Fig. 9. Measurement setup with the chip and microfluidic channel along with cell manipulation system.

Philip Feng and Hao Jia (Case Western Reserve University, Dept. ECE) for lending us the Celltram Vario system and fabricating the single cell manipulation pipette.

REFERENCES

- P. Murali, A. M. Niknejad, and B. E. Boser, "CMOS microflow cytometer for magnetic label detection and classification," *IEEE J. Solid-State Circuits*, vol. 52, no. 2, pp. 543–555, 2017.
- [2] L. Hong, H. Li, H. Yang, and K. Sengupta, "Fully integrated fluorescence biosensors on-chip employing multi-functional nanoplasmonic optical structures in CMOS," *IEEE J. Solid-State Circuits*, vol. 52, no. 9, pp. 2388–2406, 2017.
- [3] L. Hong, H. Li, H. Yang, and K. Sengupta, "Integrated angle-insensitive nanoplasmonic filters for ultraminiaturized fluorescence microarray in a 65 nm digital CMOS process," ACS Photonics, vol. 5, no. 11, pp. 4312– 4322, 2018.
- [4] M. Helou, M. Reisbeck, S. F. Tedde, L. Richter, L. Br, J. J. Bosch, R. H. Stauber, E. Quandt, and O. Hayden, "Time-of-flight magnetic flow cytometry in whole blood with integrated sample preparation," *Lab Chip*, vol. 13, pp. 1035–1038, 2013.
- [5] C. Sideris, P. P. Khial, and A. Hajimiri, "Design and implementation of reference-free drift-cancelling CMOS magnetic sensors for biosensing applications," *IEEE J. Solid-State Circuits*, vol. 53, no. 11, pp. 3065– 3075, 2018.
- [6] D. Issadore, J. Chung, H. Shao, M. Liong, A. A. Ghazani, C. M. Castro, R. Weissleder, and H. Lee, "Ultrasensitive clinical enumeration of rare cells ex vivo using a micro-hall detector," *Science Trans. Med.*, vol. 4,